Spectroscopic Studies of Model Carbonyl Compounds in CO_2: Evidence for Cooperative C−H···O Interactions

Marc A. Blatchford, Poovathinthodiyil Raveendran, and Scott L. Wallen*

Department of Chemistry, CB#3290, Kenan and Venable Laboratories, and the NSF Science and Technology Center for Environmentally Responsible Solvents and Processes, The University of North Carolina, Chapel Hill, North Carolina 27599-3290

Received: October 14, 2002; In Final Form: March 25, 2003

Acetylated carbohydrates have extremely high solubilities and miscibilities in CO_2 and form the basis of a new approach toward the development of renewable CO_2-philes. Ab initio computational studies relevant to this system indicate that in CO_2 complexes with simple, model carbonyl compounds the Lewis acid−Lewis base interaction between the carbon atom of CO_2 and the carbonyl oxygen is accompanied by a cooperative, intermolecular C−H···O interaction between the CO_2 oxygen and the solute's hydrogen atom. The results show that this may provide an additional stabilization mechanism for solvation complex formation. Spectroscopic studies provide the best approach to study these interactions and the validation of either computational or theoretical models. The present study focuses on room temperature, gaseous, liquid, and supercritical condition spectroscopic data to evaluate the extent that such complexes are relevant to CO_2 solvation. An examination of the temperature- and density-dependent changes in the vibrational spectra and the NMR shielding constants in both interacting (CO_2) and noninteracting (N_2 and He) systems supports the existence of the C−H···O interaction.

1. Introduction

Liquid and supercritical CO_2 has attracted attention as an environmentally benign solvent because of its nontoxicity, low cost, ease of removal from solutes, and recyclability. However, a large number of compounds have low solubility in CO_2, which limits the usefulness of this solvent in many applications. This has led to various molecular-level approaches to solubilize CO_2-phobic materials.[1−4] Recent ab initio calculations on the interaction of model carbonyl compounds with CO_2 indicate that these systems may offer quite interesting possibilities in terms of CO_2-philicity. In fact, the functionality predicted to have the highest interaction energy with CO_2, acetate, has been shown to allow the dissolution of carbohydrates in CO_2 upon acetylation of the hydroxyls.[5] The solvation of these compounds in CO_2 is thought to be governed principally by the interaction between CO_2 and the acetate moieties. The interaction energy for the individual acetate−CO_2 complex interaction is 2.82 kcal/mol, which presumably promotes an enthalpy-driven solvation mechanism. Understanding the fundamental solvation structures and mechanisms of these molecules is important because it will provide a systematic framework from which to approach the problem of the design of other CO_2-philes.

Although CO_2 does not possess a permanent dipole moment, it is not strictly nonpolar because there is a clear charge separation caused by the opposing bond dipoles, leaving a partial positive charge on the carbon atom and partial negative charges on the oxygen atoms.[6] CO_2 also has a quadrupole moment that causes it to interact more strongly with dipolar solutes than predicted on the basis of its dielectric constant alone.[7,8] The charge separation and quadrupole moment enable CO_2 to serve as both a Lewis acid[9,10] and a Lewis base,[5] which is recognized as being important in the CO_2-based solvation.[3,4,11,12] Energy-minimized calculations of these systems reveal that in all of the various CO_2−carbonyl interaction geometries (Figure 1) there is the possibility of a weaker, previously unknown C−H···O interaction that acts cooperatively with the Lewis acid−Lewis base interaction.

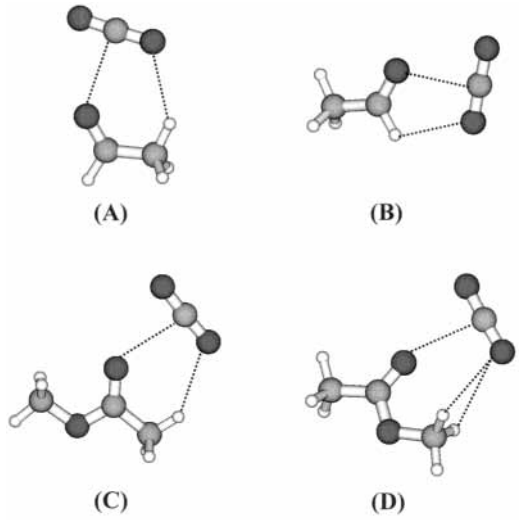

Figure 1. Optimized geometries (MP2/6-31+G*) and interaction energies (MP2/aug-cc-pVDZ) for CO_2 complexes of acetaldehyde: (A) methyl side approach ($\Delta E = -2.52$ kcal/mol), (B) aldehyde side approach ($\Delta E = -2.69$ kcal/mol) and methyl acetate, (C) methyl side approach ($\Delta E = -2.82$ kcal/mol), and (D) ester side approach ($\Delta E = -2.64$ kcal/mol).[5]

The optimized structures and binding energies suggest the existence of cyclic six-membered (CO_2−acetate) or five-membered (CO_2−aldehyde) interaction geometries involving a weak, cooperative C−H···O interaction between one of the negatively polarized CO_2 oxygens and a nearby solute proton.[5]

* Corresponding author. E-mail: wallen@email.unc.edu.

10.1021/jp027208m CCC: $25.00
Published on Web 11/07/2003

Because of the cooperativity with the Lewis acid−Lewis base interaction, it is difficult to extract the individual stabilization energies, but we have estimated the C−H···O contact to be approximately 0.5−1.0 kcal/mol in the various complexes studied. Although varying interpretations have been used to explain the nature of these weak interactions, computational and experimental studies within the past decade have provided evidence that these interactions should be viewed as nontraditional hydrogen bonds.

1.1. Nontraditional Hydrogen-Bonding Interactions. The concept of hydrogen-bonding interactions is very important in determining the organization of both inter- and intramolecular structures. In the simplest of models, a hydrogen bond is visualized as a proton donor (A−H) approaching an acceptor atom (X) containing a lone pair of electrons, resulting in the formation of a hydrogen bridge between the two species (A−H···X). The donor and acceptor atoms are usually very electronegative atoms such as oxygen, nitrogen, and fluorine. These types of interactions are traditionally thought to have a characteristic set of effects on the A−H vibrational modes that have been used to identify and characterize hydrogen-bonding interactions.[13] These classical characteristics include (1) a lengthening of the A−H bond with a corresponding red shift in the stretching vibrational mode, (2) an increase in bandwidth, (3) an increase in the infrared, but not the Raman, band intensity, and (4) a blue shift of the deformation mode with little change in bandwidth or intensity. Of these spectral features, the red shifting of the A−H stretching mode is generally considered to be the most significant indicator of hydrogen bonding. However, the concept that carbon could also participate in various degrees of hydrogen bonding and the studies performed to characterize this interaction have ultimately shown that these spectroscopic "fingerprints" are not as clearly defined as previously thought.

In 1937, Glasstone was the first to postulate that the haloform C−H bond, because of its high degree of polarity and acidity, could act as a proton donor to form a hydrogen bond.[14] At that time, this concept faced strong opposition from the majority of chemists because carbon is not a particularly electronegative atom. However, because there were indications that it could participate in hydrogen bonding if the bond was sufficiently activated, it found some small degree of skeptical acceptance. Since that time, it has been shown that these types of C−H···X bonding schemes do exist in varying degrees and play a significant role in determining molecular structure, especially in crystalline systems.[15−17] The polarity of the bond was soon recognized to play a significant role in determining the ability of the C−H moiety to be involved in hydrogen bonding. For this reason, many of the early C−H···X bonding studies primarily examined complex formation between proton acceptors, usually containing an oxygen atom, and either haloforms or other halogen-substituted species.[14,18−21] However, it was also observed in studies of alkene and alkyne derivatives[22−25] and nitrile derivatives[26−29] that the hybridization state of the carbon plays a role in C−H···X bonding, with sp > sp^2 > sp^3 in terms of hydrogen bond donor capability.

During the past several decades, there has been much discussion in the scientific community as to the exact nature of this type of interaction and the role it plays in determining structure in a variety of physical states ranging from gas- and solution-phase structures to solid-state crystal structures. In 1953, Dougill and Jeffrey speculated that the existence of a weak intramolecular C−H···O interaction involving the carbonyl and a methyl proton stabilized the dimethyl oxylate dimer.[30] Drawing upon this work, in 1963, Sutor analyzed compiled crystallographic data to postulate that C−H···X interactions could also exist in a variety of crystal structures, acting cooperatively with other stronger interactions to determine the overall molecular arrangement.[15] With this work came the realization that C−H···X interactions can occur in nonhalogenated molecules and in sp^3-hybridized carbons, although to a much lesser extent. More recently, as larger numbers of crystal structures have been determined, the relatively weak C−H···X interaction has been shown to be an important stabilizing factor in structure determination.[16,17,31−37] With the growing acceptance of the importance of C−H···X interactions in the chemical community, additional studies have also demonstrated the presence of these types of interactions in both gaseous and liquid phases.[38−43] This implies that whereas C−H···X interactions are mainly a secondary factor in overall structural geometry they may be an important stabilizing force in determining solvation structures and mechanisms.

Although it is now generally accepted that weak C−H···O interactions do occur and are important in determining chemical structure, it is still unclear as to their exact nature. Although there have been several studies that have observed the traditional red shift in the C−H stretching mode caused by the interaction's lengthening of the C−H bond,[18,22,44,45] recent ab initio calculations and experimental studies have shown that in some C−H···O interactions a contraction of the C−H bond occurs, accompanied by a blue shift in the C−H vibrational band.[46−61] Recent calculations have provided an explanation for this apparent contradiction in behavior by demonstrating that the hybridization of the carbon is important in determining not only the interaction strength but also the structural aspects of the C−H bond.[51,59,62] The chemical nature of the interaction therefore determines whether the C−H bond stretches or contracts by affecting the degree to which various chemical and electronic forces act on the bond and thus the net effect. In agreement with previous studies on sp-hybridized species that reported the classical red shifting of the C−H vibrational mode,[18,22,44,45] it was found that these interactions act analogously to the more well known O−H···O bond, showing both a lengthening of the bond and a high dependence of bond strength on intermolecular distance.[51] However, carbons possessing either sp^2 or sp^3 hybridization are affected differently. Both show a decreased dependence of bond strength as a function of intermolecular distance. Carbons having sp^2 hybridization can exhibit small degrees of either bond stretching or contraction depending on the particular type of electronegative element substitution. In all cases of sp^3-hybridized carbons studied, the bond underwent a contraction, with a subsequent blue shift of the vibrational mode. These results are corroborated by previous experimental studies that report blue shifting of the C−H vibrational mode in sp^2- and sp^3-hybridized carbons.[46−50,52,53,60]

There are two main schools of thought promulgated in the current literature regarding the nature of this blue-shifting C−H···X interaction. The first view, put forth by Hobza et al., is that blue-shifting C−H···X interactions represent a fundamentally different type of interaction having its own unique set of properties.[47−50,54,55,57,58,60] The mechanism for this interpretation involves an electron density transfer from the proton acceptor to a remote region of the donor, causing a structural relaxation that leads to the A−H bond contraction.[54] The other interpretation, suggested by Scheiner et al., is that, although shifting spectrally opposite to traditional hydrogen bonding interactions, there are no fundamental differences between C−H···X interactions and those associated with traditional

hydrogen bonding.[51,56,59,61,63] In this view, there are two sets of forces that act simultaneously on the C−H bond,[51] namely, forces that lead to bond elongation (electrostatic, polarization, charge transfer, and dispersion) and forces that lead to bond contraction (exchange). The effect on the bond is the net result of these forces. Therefore, the dominating forces in the particular type of C−H···X interaction determine whether the bond lengthens or contracts. In fact, it has been recently shown that if a strong enough dipolar interaction is present in a carbon with sp^3 hybridization then a bond elongation occurs and the traditional red shift of the C−H vibration is observed.[43]

1.2. Experimental Objectives. In agreement with previous modeling studies involving sp^2- and sp^3-hybridized carbons, the calculations for the CO_2−acetate and CO_2−aldehyde complexes predict that in all of the various geometries the C−H bond contracts because of the electron density changes from the cooperative C−H···O interaction, with a corresponding blue shift in the vibrational wavenumber.[5] Additionally, the carbonyl bond is lengthened because of the predominant Lewis acid−Lewis base interaction, and a corresponding red shift in its vibrational wavenumber is predicted. These findings have important implications for the proposed CO_2-solvation mechanism of acetylated sugars or of acetate-containing compounds in general. In enthalpic terms, if solvation of the acetate functionalities with CO_2 through the Lewis acid−Lewis base interaction sufficiently disrupts the solute−solute interactions, then the compound is solubilized. Compounds with a high degree of acetylation exhibit enhanced CO_2 solubility.[12] Therefore, whereas the secondary, cooperative C−H···O interaction is relatively weak, it may help to explain this higher degree of CO_2 solubility in acetate-containing compounds. The goals of the present study are to characterize the thermodynamic dependence (pressure and temperature) of vibrational modes and NMR chemical shifts of simple, model CO_2-philic compounds (methyl acetate and acetaldehyde) and to examine spectroscopic evidence for the presence of the cooperative C−H···O interaction.

2. Experimental Section

2.1. Reagents. Helium (Holox), nitrogen (National Welders' Supply Co.) and SFE-grade carbon dioxide (Scott Specialty Gases, Inc.) were used as received. Acetaldehyde (99.5%, Aldrich Chemical Co.) and methyl acetate (99.5%, Aldrich Chemical Co.) were dried over activated 4-Å molecular sieves (Fisher Scientific) prior to use.

2.2. General Experimental and Analysis Methods. For comparison purposes in all studies, pressurized He and N_2 were used as nonspecifically interacting reference gases (only dispersive interactions present). Gas densities were determined at the various pressures by using equation-of-state data provided through the NIST database as previously described.[64] Vibrational data were processed, and peaks were fit to Lorentzian bands using standard analysis software (Galactic, Grams/32).

2.3. Raman Instrumentation and Method. The Raman experimental setup using the high-pressure Raman NMR (HPRNMR) cell was described previously.[65] Liquid methyl acetate or acetaldehyde was mixed with pressurized gas in an external pressure vessel. The headspace gas containing the analyte vapor was then bled into the spectroscopic cell. All Raman measurements were made using an Ar^+ laser (Spectra Physics Model 2020-05), operating at 60 mW on the 514.5-nm line. Plasma lines were removed from the beam by filtering through a Pellin-Broca prism system with a spatial filter. Temperature control was achieved using a homemade copper heating element regulated by a PID controller (Omega Engineering CN76000) and measured using a 100 W platinum RTD (Omega Engineering, Inc.). All data in the Raman studies were collected at 25.0 ± 0.2 °C. Pressures were generated using a manual high-pressure syringe pump (HIP model 50-6-15) in the He and N_2 studies and an automated syringe pump (ISCO model 100DX) in the CO_2 studies. Pressures were measured with a Bourdon-type gauge (Heise H43315) with uncertainties of ±0.3 bar. Raman scattered light, using a 90° collection geometry, was sent through a 1.0-m additive double monochromator (Jobin-Yvon U1000) with 1800-groove density gratings. The entrance slit was set at a width of 20 μm and a slit height of 2 mm. Each spectrum was acquired over a 10-min integration time using a liquid-nitrogen-cooled CCD camera (Princeton Instruments NTE-400EB). Spectra were subsequently calibrated using the Ar^+ laser plasma lines using the method of Carter et al.[66] Cosmic rays were removed, and the spectra were background corrected using standard analysis software (Galactic, Grams/32).

2.4. FTIR Instrumentation and Method. All FTIR experiments were performed using a Thermo Nicolet Magna-IR 750 spectrometer. The experimental setup was modified slightly by replacing the HPRNMR cell with a stainless steel viewcell containing opposed diamond windows. A smoothing algorithm in the spectrometer software (Nicolet, Omnic v5.1) was applied to the resulting FTIR spectra to eliminate interference fringe patterns caused by the diamond windows. All data were the average of 64 transients. Temperature control was achieved using a circulating 1:1 H_2O/ethylene glycol bath (Neslab RTE-210) that was pumped through copper tubing in contact with the cell while the cell temperature was monitored using a platinum RTD. For low-density and preliminary spectral shift studies, liquid methyl acetate or acetaldehyde was mixed with the pressurized gas in an external pressure vessel. The headspace gas containing the analyte vapor was then bled into the spectroscopic cell, which was isolated from the rest of the pressure system. For condensed-phase CO_2 studies, a known amount of acetate was injected directly into the spectroscopic cell and subsequently pressurized. For carbonyl band and C−H stretching-band observations, 16.0 μL ($\chi_{MeOAc} = 0.001$) and 80.0 μL ($\chi_{MeOAc} = 0.005$) of methyl acetate were used, respectively. A higher concentration of methyl acetate was used for the C−H studies to increase the S/N ratio of the bands. The corresponding mole fractions were calculated using the known volume of the cell (9.6 mL) and values of CO_2 density (ρ) at the initial pressure and temperature. Solute mole fractions were kept low to approximate infinite dilution conditions and to minimize the degree of solute−solute interactions. Experiments were performed by beginning at the highest density and systematically reducing the pressure through a restrictor to maintain constant mole fraction conditions, except in the study with increasing concentration of CO_2.

2.5. NMR Instrumentation and Method. NMR experiments were conducted using the HPRNMR cell. Liquid methyl acetate or acetaldehyde was mixed with the pressurized gas in an external pressure vessel. The headspace gas containing the analyte vapor was then bled into the spectroscopic cell, which was isolated from the rest of the pressure system. All experiments were performed by beginning at the highest density and systematically reducing the pressure through a restrictor to maintain constant mole fraction conditions. Measurements were made using a 5 mm HF probe on a Bruker Avance spectrometer equipped with an 11.75-T superconducting magnet operating at 500.1 MHz for the ^1H nucleus. No lock solvent was used in these experiments because the magnetic field in the detection

TABLE 1: Summary of the Observed Vibrational Bands at 25.0 °C under Isodensity (2.38 mol/L) Conditions[a]

mode assignment	Raman (cm^{-1}) He	Raman (cm^{-1}) N_2	Raman (cm^{-1}) CO_2	FTIR (cm^{-1}) He	FTIR (cm^{-1}) N_2	FTIR (cm^{-1}) CO_2
			Acetaldehyde			
C═O symmetric stretch	1745.8	1744.9	1743.9	1745.4	1743.7	1739.0
aldehyde symmetric stretch	2716.5	2716.2	2717.3			
aldehyde symmetric stretch	2718.2	2718.2	1721.2			
			Methyl Acetate			
C═O symmetric stretch	1770.3	1768.9	1767.0	1777.7	1777.6	1776.1
C═O symmetric stretch	1769.0	1766.9	1762.2	1762.1	1761.2	1760.6
symmetric CCH_3	2952.7	2952.1	2951.8			
symmetric OCH_3	2964.7	2963.9	2964.1	2964.0	2963.6	2963.1
asymmetric CH_3 stretch				3020.2	3021.9	3031.4
antisymmetric CH_3 stretch				3002.1	3001.3	3004.5

[a] Required pressures are 60.6, 58.9, and 43.4 bar for He, N_2, and CO_2, respectively.

region does not drift appreciably during the duration of the experiment. Spectra were collected using a 30° pulse program as the average of 24 transients at each pressure point. All experiments were performed at 25.0 ± 0.1 °C and controlled using the air bath and temperature controller (Eurotherm BVT3000) provided with the spectrometer. Chemical shifts were referenced to the zero-density value for each system studied.

3. Results and Discussion

3.1. Vibrational Spectroscopy. Pressure changes cause broadening and wavenumber shifts in vibrational bands. These changes are a convolution of specific intermolecular interactions and changes in ρ due to dielectric changes and dispersion interactions. Therefore, to determine the extent of the changes caused by solvent ρ and thus determine the existence of any specific interactions, the spectroscopic results for CO_2 must be compared to a gas in which no specific interactions are present. For this purpose, He and N_2 were chosen, each representing a different degree of nonspecific interaction. Because He is a very small, weakly polarizable atom, the most significant intermolecular interactions are the weak van der Waals and induced dipole forces. N_2, however, is more polarizable than He and has a π-electron system that is capable of weakly interacting with the carbonyl groups of methyl acetate and acetaldehyde, leading to overall larger intermolecular forces. By comparing the results for these two gases to the results obtained for CO_2, we should be able to observe three different scenarios: (1) the spectral behavior of the solute in the absence of any significant intermolecular interaction (He), (2) the spectral behavior of the solute with weak intermolecular interactions (N_2), and (3) the spectral behavior of the solute in the presence of stronger intermolecular interactions and possibly a specific C−H···O interaction (CO_2). The isodensity Raman and FTIR results for acetaldehyde and methyl acetate are shown in Figures 2−5, respectively, with a tabulated summary of assignable band positions presented in Table 1.

3.1.1. Acetaldehyde−CO_2. Carbonyl Stretch. As shown in Figures 2A and 3A, the carbonyl vibrational band of acetaldehyde in N_2 broadens and slightly red shifts (−0.92 cm^{-1} in the Raman spectrum and −1.75 cm^{-1} in the FTIR spectrum) compared to its position in He. The red shift can be interpreted as the existence of a weak intermolecular interaction. Although the bands are slightly shifted, the overall band structure does not change significantly in appearance or spectral bandwidth, indicating very weak intermolecular interactions that do not affect the strength of the vibrational mode or relaxation dynamics. In the presence of CO_2, however, the carbonyl band significantly broadens and red shifts compared to the bands in both N_2 and He. This shift can be directly attributed to the Lewis acid−Lewis base interaction between acetaldehyde and CO_2. The broadening appears to be inhomogeneous in nature and is primarily toward the low-energy side of the band. It is also interesting that the carbonyl FTIR band change from split bands in He to a single, lower-energy band in CO_2. This appears to be due to both the collapse of the rovibrational P and R branches into the central Q branch and a shifting in equilibrium between the uncomplexed and complexed states in the presence of the CO_2 interaction. This complexation equilibrium will be discussed in more detail in the section regarding the methyl acetate−CO_2 complex.

Aldehydic Proton. Acetaldehyde provides a unique case for analysis in the gas phase. As shown in Figure 1, one calculated geometry involves the CO_2 interacting with the methyl protons whereas the other places the interaction at the aldehydic proton. The aldehydic proton has a vibrational mode at 2717 cm^{-1} that is distinct from that of the other protons, making it easier to observe and analyze. Figures 2B and 3B show the Raman and FTIR results for this vibration, respectively. The Raman spectral band is satisfactorily fit to two Lorentzian bands. The band in N_2 is slightly red shifted from its position in He with little change in the overall band profile. In the CO_2 spectrum, however, the bands are significantly broadened, decrease in intensity, and are now blue shifted 0.8 and 3.0 cm^{-1} from their positions in He, respectively.[67] This broadening and intensity decrease in aldehydic proton vibrational bands has been previously ascribed to intermolecular C−H···O interactions.[68,69] The FTIR spectra in this region are too complex for peak-fitting analysis because of interference from the presence of Fermi resonance and combination bands. However, the shoulder due to the aldehydic proton can be qualitatively observed. This band appears to broaden and blue shift in CO_2 compared to He, causing it to merge with the Fermi resonance band, becoming a poorly resolved shoulder. The blue shift of the aldehydic proton is predicted from the geometry in which CO_2 forms a C−H···O interaction with this proton (Figure 1D).

What is also interesting is the opposite behavior observed for the aldehydic proton between N_2 and CO_2 compared to He (Figures 2B and 3B). When N_2 is used as the pressurizing medium, the band shape remains relatively unchanged, showing a slight red shift in its Raman position and no observable shift in its FTIR position. When CO_2 is used, there is a dramatic effect on the band shape and position, showing that there is a fundamentally different kind of interaction taking place. The band now blue shifts and becomes significantly broadened toward the blue edge, again indicative of the C−H···O interaction. Methyl acetate and acetaldehyde should have only weakly polarizing intermolecular interactions with N_2, possibly the overlap of the π-electron systems of the carbonyl and the N_2

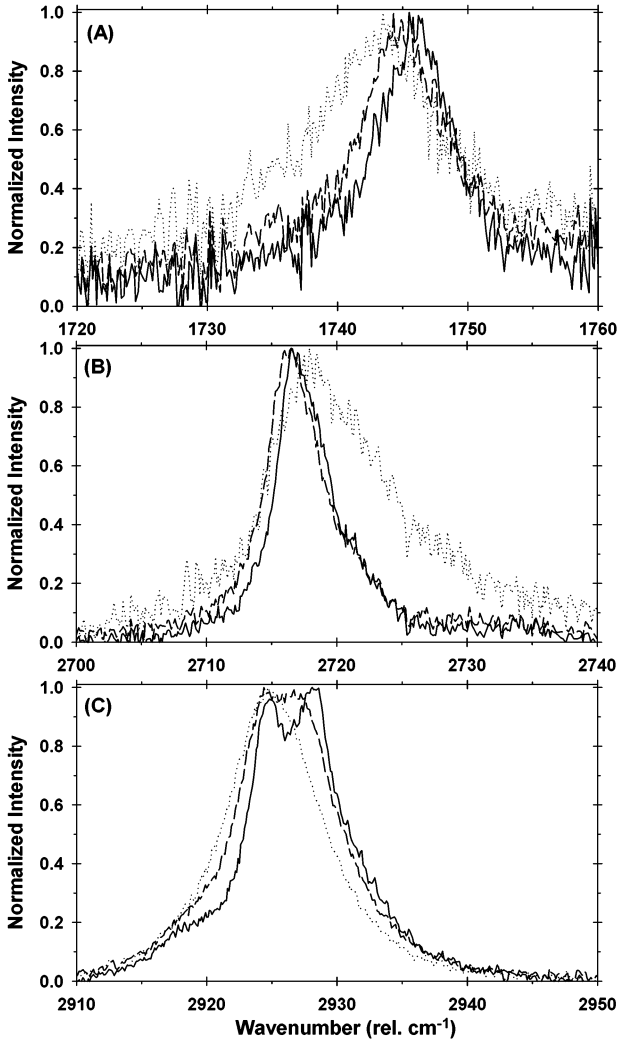

Figure 2. Raman spectra of acetaldehyde pressurized at 25.0 °C in isodensity (2.38 mol/L) He (60.6 bars, —), N_2 (58.9 bars, − − −), and CO_2 (43.4 bars, ···) in the (A) carbonyl, (B) aldehyde proton, and (C) methyl proton regions.

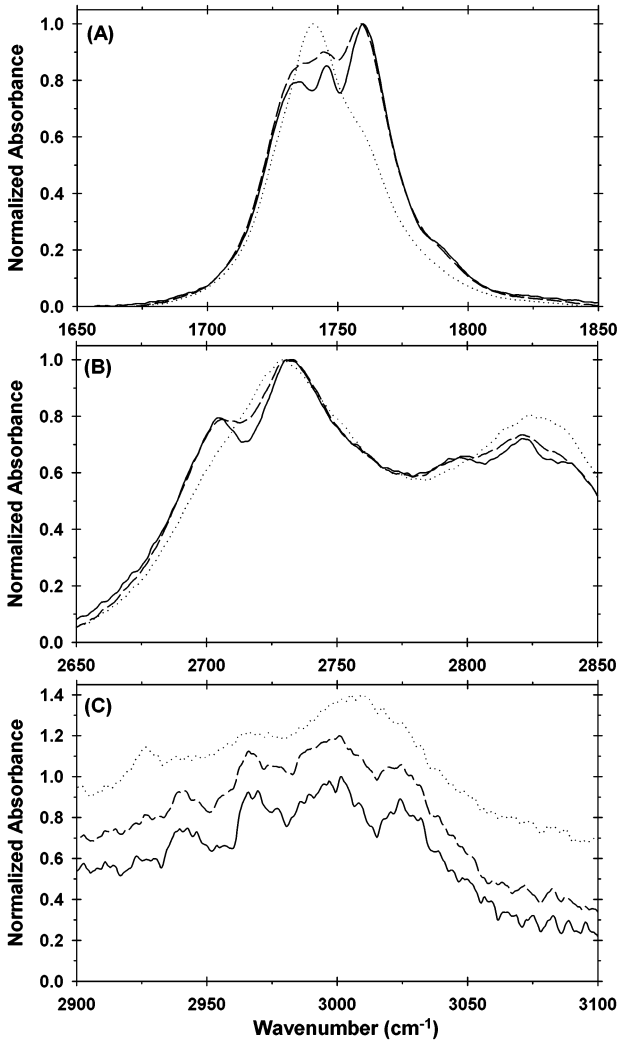

Figure 3. FTIR spectra of acetaldehyde pressurized at 25.0 °C in isodensity (2.38 mol/L) He (60.6 bars, —), N_2 (58.9 bars, − − −), and CO_2 (43.4 bars, ···) in the (A) carbonyl, (B) aldehyde proton, and (C) methyl proton regions. Spectra in (C) have been offset for clarity.

molecule. Because this interaction geometry is perpendicular to the carbonyl vibrational motion and does not directly interact with either of the atoms, it would not have a profound dampening effect on the vibration or affect the vibrational dephasing times as strongly. This causes the peak width to remain relatively unchanged. The added electron density in the carbonyl π system would qualitatively predict that the bond would be weakened, causing this vibration and any vibration directly coupled to the carbonyl, such as that of the aldehyde proton, to shift to slightly lower wavenumbers. These effects could also be observed in the presence of a weaker C−H···π interaction between the two molecules. The significant broadening of both the carbonyl and aldehydic proton bands in the presence of CO_2 indicates a much different type of interaction. Unlike N_2, CO_2 can act as a Lewis acid forming an interaction complex with a lone pair of electrons on the carbonyl oxygen. In this case, the interaction occurs within the vibrational plane and involves a direct interaction with one of the atoms in the bond. This causes a dramatic dampening effect on the vibrational motion. The dampening not only causes the carbonyl vibration to shift to lower wavenumbers but also can profoundly shorten the vibrational dephasing time, causing the band to broaden and decrease in overall intensity. As the Lewis acid−Lewis base interaction orients the CO_2 into the correct geometry to form the cooperative C−H···O interaction with the aldehydic proton, the lone pair of electrons on the CO_2 oxygen atom directly interacts with the hydrogen in the plane of the C−H bond. This shortens the vibrational dephasing time of the mode, causing the observed band to broaden and decrease in intensity. The only difference is that now the net electronic forces in this interaction induce the bond to contract rather than elongate, and the vibration is shifted to higher wavenumber (blue shift).

Methyl C−H Stretch. The main bands visible in the Raman spectra are due to the symmetric vibrational modes. Both bands red shift slightly in the presence of CO_2. This result is counter to the predicted result from the ab initio calculations, which predict all blue shifts of the various C−H stretching modes. The asymmetric and antisymmetric C−H stretching bands in the FTIR spectra, although remaining relatively unchanged in the presence of N_2, appear to blue shift in the presence of CO_2 (Figure 3C). Although the bands are too weak and highly overlapped to perform a reliable peak-fitting analysis, the peak that appears at ∼3000 cm^{-1} can be clearly seen to blue shift in the CO_2 spectrum compared to those in the N_2 and He spectra. This latter result is consistent with the predicted spectral shifts for the C−H···O interaction.

3.1.2. Methyl Acetate−CO_2. Carbonyl Stretch. As shown in Figures 4A and 5A, the carbonyl vibrational band in methyl

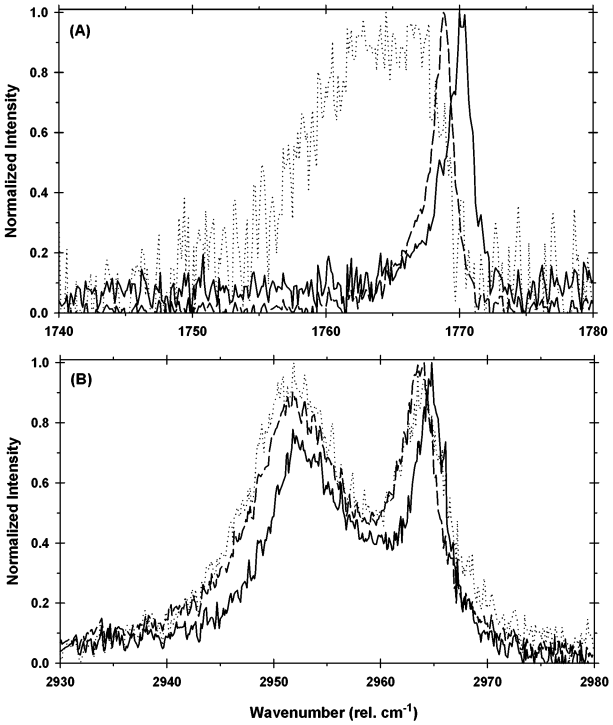

Figure 4. Raman spectra of methyl acetate pressurized at 25.0 °C in isodensity (2.38 mol/L) He (60.6 bars, —), N_2 (58.9 bars, – – –), and CO_2 (43.4 bars, ···) in the (A) carbonyl and (B) methyl proton regions.

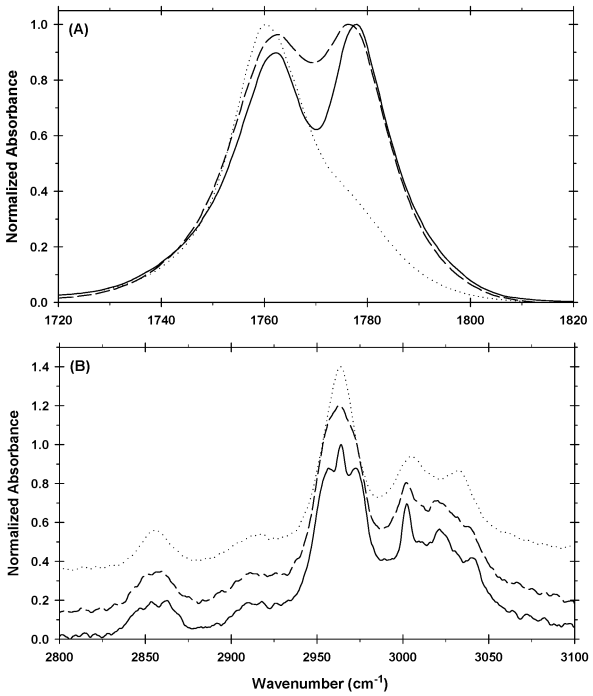

Figure 5. FTIR spectra of methyl acetate pressurized at 25.0 °C in isodensity (2.38 mol/L) He (60.6 bars, —), N_2 (58.9 bars, – – –), and CO_2 (43.4 bars, ···) in the (A) carbonyl and (B) methyl proton regions. Spectra in B have been offset for clarity.

acetate in N_2 slightly red shifts from those in He, similar to the shifts observed for acetaldehyde. Again, the overall band structure does not appreciably change in appearance or spectral bandwidth, indicating the presence of very weak intermolecular interactions (van der Waals forces) that do not significantly affect the nature of the vibrational motion or the dynamics. In CO_2, the carbonyl band significantly broadens and red shifts compared to the band in both N_2 and He, as observed in acetaldehyde. This shift can again be explained as a direct result of the Lewis acid−Lewis base interaction between methyl acetate and CO_2. The FTIR bands of the carbonyl also change from split bands in He to a single, lower-energy band in CO_2 (Figure 5A). In the acetaldehyde spectrum, this appears to be mainly due to the collapse of the rovibrational P and R branches into the central Q branch in the presence of the CO_2 interaction. However, the situation for the two bands observed in the methyl acetate spectrum is slightly more complex. Two bands in the carbonyl region have previously been interpreted as the simultaneous occurrence of a monomeric species and the dimeric complex of the solute.[69,70] In CO_2, the relatively strong Lewis acid−Lewis base interaction drives the monomer concentration down as the pressure is increased and causes an increase in the concentration of the complexed state. In the present case, the lower-wavenumber band is interpreted as the pressure-driven formation of CO_2−methyl acetate complexes rather than methyl acetate−methyl acetate dimers. This can be verified by observing the FTIR carbonyl band as a function of CO_2 pressure. The results from these experiments are presented in Figure 6.

Figure 6A and B shows the changes occurring in the carbonyl band as a function of pressure under constant $\chi_{MeOAc} = 0.001$ conditions in He and CO_2, respectively. In He, the appearance of the band remains relatively unchanged as a function of pressure, with the band area ratio remaining fairly constant (<10% change). This indicates that there is no significant interaction taking place between methyl acetate and He and that the reaction volume of the monomer−dimer reaction is relatively low, meaning much greater pressures are necessary to shift a significant fraction of the monomer to the dimeric form. Although the data are not shown, similar results are obtained for methyl acetate in pressurized N_2. In CO_2, however, the band shape changes dramatically as a function of pressure. As the pressure is increased, the 1778-cm^{-1} monomer band decreases in intensity while the 1761-cm^{-1} "complex" band increases, as shown by the decreasing area ratio determined from the integrated peak areas. The increased intensity observed for the lower-wavenumber band is not attributable to a shifting of monomeric to dimeric methyl acetate but rather to a conversion from monomeric methyl acetate to the CO_2−methyl acetate complex.

In pressurized He, no significant interaction takes place between the gas and methyl acetate, so the only contributions to the observed band shape come from the monomeric and dimeric methyl acetate species. In CO_2, however, the spectra are further complicated by the possibility of a CO_2−methyl acetate mixed dimer complex. Figure 6C illustrates the results of increasing the amount of CO_2 with a given amount of methyl acetate. The observed pressure dependence of these spectra reveals that a CO_2−methyl acetate mixed dimer is the prominent species under higher CO_2 pressures. Because increased dimer formation would be thermodynamically unfavorable with increasing dilution, the only reasonable explanation for the increase in the lower-wavenumber band is the formation of a methyl acetate−CO_2 mixed dimer complex. Evidence of this comes from previous dilution studies,[69,70] which indicate that the monomer−dimer equilibria of carbonyl compounds in CCl_4 favor the monomeric state as the solute becomes increasingly dilute. Because there is no significant shift of the higher-wavenumber band position even at relatively high CO_2 pressures, we presume that there is no noticeable shift in the CO_2−methyl acetate mixed dimer band compared to that of the methyl acetate dimer. It is plausible that carbonyl band positions for the methyl acetate dimer and methyl acetate−CO_2 dimer are

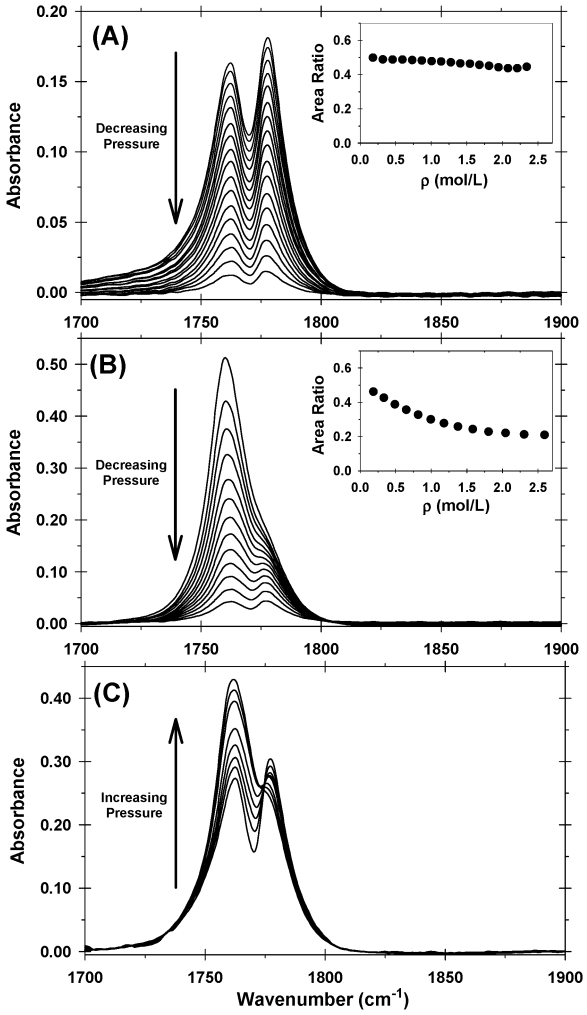

Figure 6. FTIR spectra of methyl acetate as a function of pressure at 25.0 °C in (A) He (59.6−4.4 bars) and (B) CO_2 (45.8−4.4 bars). (C) Results of diluting a fixed amount of methyl acetate with CO_2 at 25.0 °C.

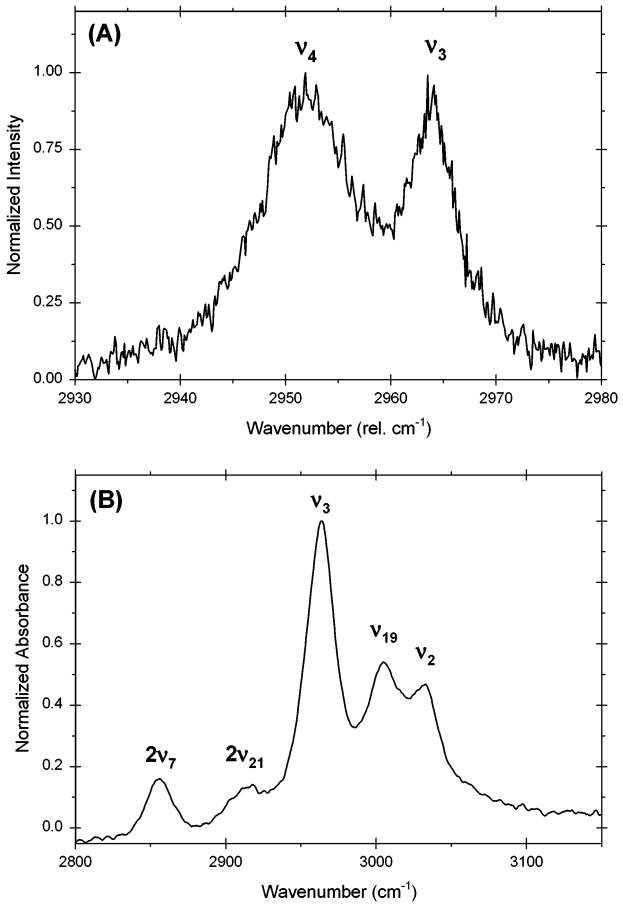

Figure 7. (A) Raman spectrum of methyl acetate in the methyl proton region. (B) FTIR spectrum of methyl acetate in the methyl proton region. Both spectra are in CO_2 at 25.0 °C and 45.9 bars. See Table 2 for vibrational mode assignments of the main bands from the literature.[72] $2\nu_{21}$ and $2\nu_7$ are C−CH_3 deformation overtones.

inseparably close because the dimer and the mixed dimer both involve Lewis acid−Lewis base interactions of the carbonyl group. It may be concluded that there is a shift in the equilibrium toward the methyl acetate−CO_2 dimer at higher CO_2 pressures, as predicted for complex formation by Le Chatlier's principle.

Methyl C−H Stretch. The interpretation of the methyl proton stretching region is more complicated than that of the carbonyl and aldehydic proton regions. There is a high degree of band overlap in this region, which makes the peak-fitting analysis rather complex. In the He and N_2 spectra, the rovibrational structure of the bands is present. However, all rovibrational structure appears to collapse into a single band in CO_2. Although this collapse is evidence for significant intermolecular interactions in CO_2,[71] the presence of these rovibrational sidebands in the He and N_2 spectra makes them more difficult to assign and analyze. It is important to note that in sp^2- and sp^3-hybridized carbons the observed changes in bond length, and thus in vibrational wavenumber, are very small and are at best ambiguous, depending on the nature of the electronegative substituents on the molecule.[59] Therefore, the absence of a significant shift in a vibrational mode, although not providing evidence for the existence of a C−H···X interaction, can also not conclusively exclude it. In addition, from the calculated optimized geometries, it can be seen that two main cooperative interaction configurations are possible (Figure 1C and 1D). CO_2 can form cooperative C−H···O interactions of nearly equal energies with the methyl protons on either the acetate methyl or ester methyl group (2.82 and 2.64 kcal/mol, respectively).[5] Because these geometries have nearly the same interaction energies, enthalpic considerations of the Boltzmann distribution predict that there should be approximately equal populations between the two possible configurations, each having its own unique spectral contribution that is averaged in the resultant spectrum. Because the C−H···O interaction is also very weak, it does not lock the methyl groups into one particular spatial configuration in the room-temperature solution structure. Therefore, the resulting vibrational spectrum will be an average of the distribution of possible complexation geometries and methyl rotational states, making it more difficult to directly compare the observed spectral bands to the wavenumbers predicted by ab initio calculations for the various geometries.

Methyl acetate spectra in the C−H stretching region are shown in Figures 4B and 5B. As discussed, this region is fairly complex, with many overlapping bands and rovibrational structures. However, previous work has established the assignment of the vibrational bands.[72,73] Figure 7 shows the Raman and FTIR spectrum of methyl acetate in CO_2 with vibrational mode assignments obtained from the literature. Both symmetric stretching bands in the Raman and FTIR spectra red shift slightly in the presence of both N_2 and CO_2, which is counter to the results expected for the cooperative C−H···O interaction. However, the asymmetric and antisymmetric C−H stretching bands in the FTIR spectra, although remaining relatively

TABLE 2: Summary of ab initio (MP2/6-31+G*) Vibrational Wavenumbers for the Uncomplexed Methyl Acetate (MeOAc) and the MeOAc−CO_2 Complexes in the Methyl Side and Ester Side Approaches[5]

vibrational mode	assignment	isolated MeOAc (cm^{-1})	methyl side geometry (cm^{-1})	ester side geometry (cm^{-1})
ν_1	antisymmetric C−CH_3 stretch	3240.3	3244.3	3241.0
ν_2	antisymmetric O−CH_3 stretch	3254.0	3255.4	3258.7
ν_3	symmetric O−CH_3 stretch	3125.9	3127.3	3132.9
ν_4	symmetric C−CH_3 stretch	3119.1	3118.8	3118.3
ν_5	C═O symmetric stretch	1792.0	1786.0	1785.1
ν_{18}	asymmetric C−CH_3 stretch	3204.6	3203.1	3203.2
ν_{19}	asymmetric O−CH_3 stretch	3222.9	3225.2	3233.9

unchanged in the presence of N_2, blue shift by 2.3 and 11.1 cm^{-1}, respectively, in the presence of CO_2. This latter result is consistent with the predicted spectral shifts for the C−H···O interaction. The rovibrational structure can also be used to demonstrate the extent of the molecular interactions present in CO_2 compared to those in He and N_2. As clearly seen in Figure 5B, there are prominent rovibrational bands in both the He and N_2 spectra. However, in CO_2, these structures completely collapse, indicating the presence of a specific intermolecular interaction.[71]

3.1.3. Gaseous CO_2 Environment. Although the preliminary spectral investigation has provided many results consistent with the presence of the C−H···O interaction, a more in-depth thermodynamic examination of the methyl proton stretching region in CO_2 to study the effects of CO_2 solvation is warranted. Only methyl acetate was explored in all of these studies for two reasons: the FTIR bands of methyl acetate have greater intensity than those of acetaldehyde in the C−H stretching region, and acetaldehyde shows evidence of polymerization after several minutes in the spectroscopic cell. FTIR studies were conducted at various temperatures to examine the relevance of these interactions over the entire range of conditions in which CO_2 is utilized industrially. As illustrated in Figure 7B, the methyl acetate FTIR spectrum in this region can be fit to five different bands corresponding to ν_1/ν_2, ν_{18}/ν_{19}, ν_3, $2\nu_{21}$, and $2\nu_7$. The predicted vibrational shifts from the ab initio calculations are summarized in Table 2.

The ν_4, ν_{18}, and ν_1 bands of methyl acetate correspond to the respective symmetric, asymmetric, and antisymmetric C−H modes of acetate methyl whereas the ν_3, ν_{19}, and ν_2 bands correspond to the respective ester methyl modes. The vibrational modes from methyl groups in close proximity to carbonyl functionalities are known to give rise to very weak infrared absorptions.[74] Previous work on deuterated analogues of methyl acetate have shown that in the vibrational modes consisting of ν_1/ν_2 and ν_{18}/ν_{19}, the ν_2 and ν_{19} components are responsible for the majority of the signal observed in the C−H stretching region.[72] In fact, the examination of FTIR spectra of a deuterated analogue gave analogous results to those reported here with the protonated form. In the discussion, we will discuss ν_1/ν_2 and ν_{18}/ν_{19} in terms of the major components because the minor components do not improve the fits or substantially change the resulting trends. For all data acquired in these experiments, the resulting spectra were fit to five bands corresponding to the three ester methyl vibrational modes, ν_3, ν_{19}, and ν_2, and two C−CH_3 deformation overtones, $2\nu_{21}$ and $2\nu_7$.

The first experimental condition examined as a function of pressure was in the gaseous CO_2 phase region at ambient temperature (25.0 °C), and the results are presented in Figure 8. As predicted by ab initio calculations, both the ν_2 antisymmetric and ν_{19} asymmetric bands appear to blue shift as pressure increases,[5] causing the equilibrium to shift more toward complex formation. Additionally, the ν_3 symmetric band is shown to red shift slightly at these lower-pressure conditions. Although the ab initio calculations predict that the ν_4 band (symmetric C−CH_3 stretch) should red shift slightly, the ν_3 mode is predicted to blue shift similarly to the asymmetric and antisymmetric modes.

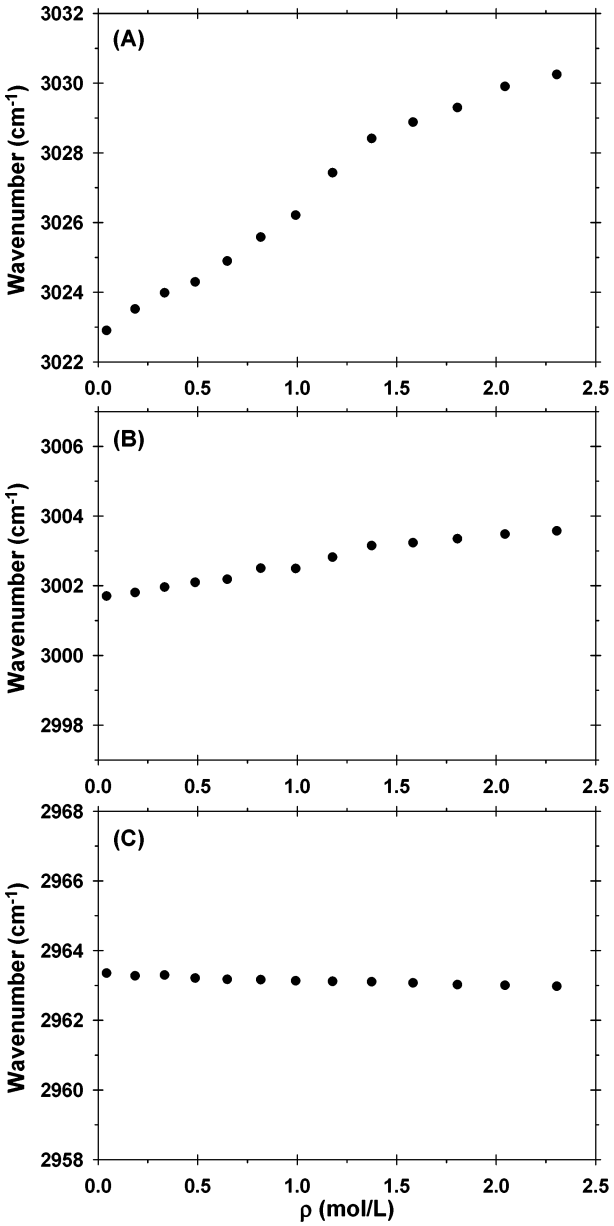

Figure 8. Figure 8. Plots of FTIR vibrational mode peak position as a function of pressure (45.8−1.0 bars) in gaseous CO_2 at 25.0 °C. (A) ν_2, (B) ν_{19}, and (C) ν_3.

3.1.4. Supercritical CO_2 Environment. The next set of experiments extends the study into the supercritical region (40.0

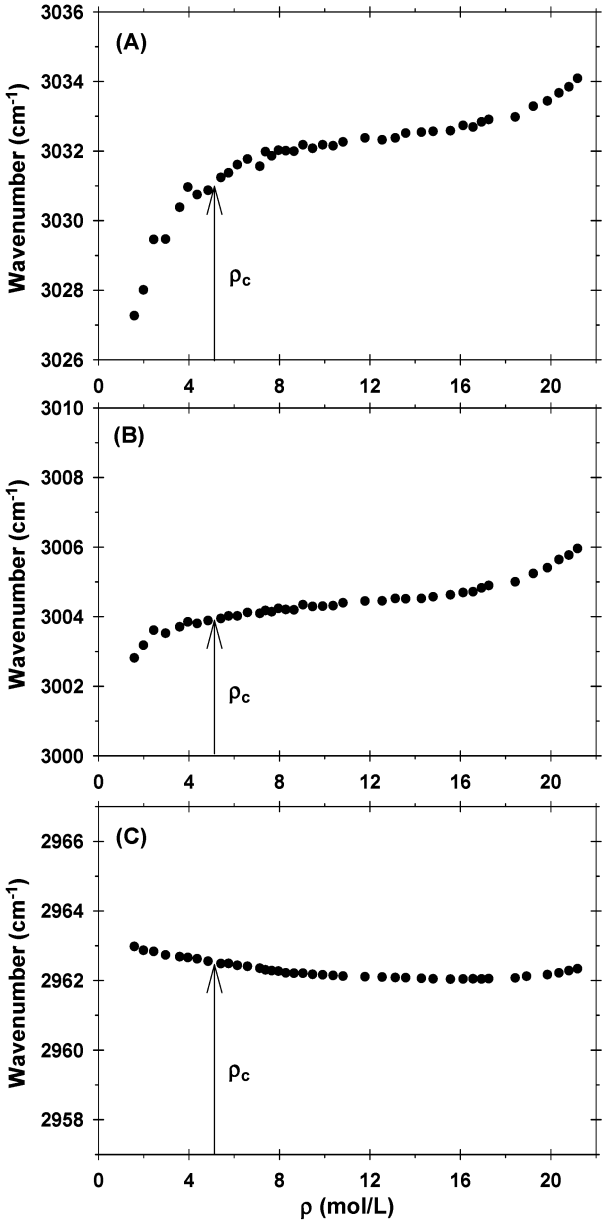

Figure 9. Plots of FTIR vibrational mode peak position as a function of pressure (345.7−35.4 bars) in supercritical CO_2 at 40.0 °C. (A) ν_2, (B) ν_{19}, and (C) ν_3. The unmodified critical density (ρ_c) for CO_2 is indicated with an arrow.

°C) of the CO_2 phase diagram, and the results are presented in Figure 9. As in the 25.0 °C experiment, both the ν_2 antisymmetric and ν_{19} asymmetric bands appear to blue shift steadily as pressure increases, with a leveling of the trend as the system makes the transition between the gaseous and supercritical states near the critical pressure (5.11 mol/L). Previous studies by Fayer et al. attribute such behavior to critical clustering of the solvent around the solute molecule.[75−77] It is possible that similar clustering could be present in systems that presumably contain such CO_2 complexes as those discussed. However, we will not explore this issue in the present study. The ν_3 band is interesting. As in the ambient-temperature study, the band slightly red shifts as the pressure increases; however, once the CO_2 enters the supercritical regime, the vibrational wavenumber levels to a constant value, and then the band begins to blue shift at higher densities. The results in the higher-density region are consistent with the blue-shifting trend predicted for this mode in the ab initio calculations. However, the initial red shift in wavenumber here and in the gaseous CO_2 study cannot be interpreted using the present model.

3.1.5. Isodensity Variable-Temperature Study. As previously discussed, the observed vibrational spectra are an averaged convolution of a distribution of states with various populations. Because the C−H···O interactions are very weak (<1 kcal/mol) and on the order of *kT* at ambient conditions, the inherent kinetic motion of the molecules is sufficient to overcome the enthalpic portion of the interaction, causing the solvent−CO_2 complexes to distribute themselves dynamically among the various interaction geometries. In addition, the internal rotation about the chemical bonds in the solvent molecule causes the C−H···O interaction to be averaged equally among all of the protons. These two factors cause the overall effect experienced by the protons to be less than if the molecules were locked into a specific interaction geometry. However, as the system is cooled and the internal energy is decreased, the molecular kinetic motion is slowed, and the molecules no longer possess sufficient energy to redistribute themselves among the various states. Therefore, as the temperature is lowered, the weak C−H···O interactions should become more significant with respect to *kT*, and the protons begin to experience a greater effective interaction force. Another view of this is that as the population exchange-rate slows the bands should begin to narrow and shift more toward wavenumbers and band shapes that are indicative of the specific type of interactions present. To explore this phenomenon, studies were conducted as a function of temperature in condensed-phase CO_2 at a constant density (22.35 mol/L). The results from this study are presented in Figure 10. Both the ν_2 antisymmetric and ν_{19} asymmetric C−H modes (Figures 10A and B) blue shift as temperature decreases, which is again in qualitative agreement with the behavior predicted from the calculations for the presence of a cooperative C−H···O interaction. As in the previous studies, the ν_3 symmetric mode (Figure 10C) mode exhibits anomalous behavior and remains relatively constant as a function of temperature. As shown in Figure 11A and B, the carbonyl band exhibits the expected red shifting associated with the Lewis acid−Lewis base interaction in both the supercritical and isodensity temperature experiments.

3.2. NMR Spectroscopy. NMR chemical shifts (δ) are determined by local electronic structure within a molecule, and the measurements of these shifts can be used to provide a detailed view of solvation effects. Shifts in electron density result in perturbations of the chemical shielding tensor, which in turn affect the observed value of δ. Because hydrogen bonding causes changes in electronic structure, δ measurements are a sensitive probe of the local electronic environment experienced by each nucleus upon bond formation. At the molecular level, the magnetic shielding constant (σ) is sensitive to the chemical environment, providing an absolute measure of the electronic contribution to the observed nuclear magnetic moments.[78] When the cooperative C−H···O interaction is formed in the complex, interaction of the methyl hydrogen with the lone pair of electrons on the CO_2 oxygen atom causes a polarization in the molecular orbitals, resulting in an electron density shift in the region around the C−H bond. This is the main phenomenon responsible for causing the stretching and/or contraction in hydrogen-bonded species as well as the changes in vibrational wavenumbers and band shapes. NMR spectroscopy is ideally suited for studying these electronic redistribution effects. Because the σ of a particular proton is a measure of the net magnetization experienced by that proton from the local electron cloud density, this value is extremely sensitive to changes in electron density. Therefore, if a cooperative C−H···O interaction occurs in the

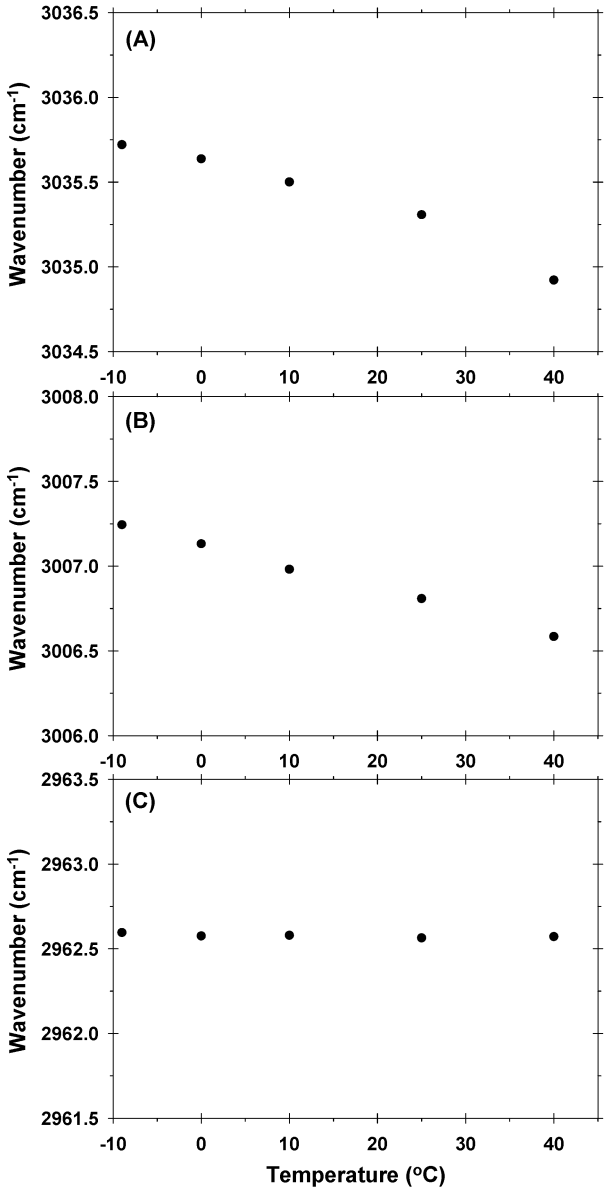

Figure 10. Plots of FTIR vibrational mode peak position as a function of temperature (−10.0 to 40.0 °C) in liquid CO_2 at constant density (22.35 mol/L). (A) ν_2, (B) ν_{19}, and (C) ν_3.

CO_2−acetate complex, then the electron density shift caused by the interaction should be measurable using NMR.

σ is a second-order molecular property that is usually expanded in terms of ρ using the following virial expansion:

$$\sigma(T, \rho) = \sigma_0(T) + \sigma_1(T)\rho + \sigma_2(T)\rho^2 + ... \quad (1)$$

σ_0 is the contribution from the rotational and vibration intramolecular dynamics of the isolated gas molecule, σ_1 is an approximate measure of the effects of pairwise interactions, and σ_2 is due to the effects of multibody interactions. Previous studies have shown that the linear terms are generally sufficient to describe the shielding as a function of density for lower densities (<2.5 kbar).[79−82] At higher densities, however, deviation from linear dependence was observed, and the higher-order terms of eq 1 were necessary. In the current study, we assume that the linear term in the virial expansion is sufficient to describe the solvent−solute intermolecular interactions. Because the observed chemical shift (δ_{obs}) and σ differ only by an additive constant, the chemical shift relative to an isolated molecule can be written in terms of the individual contributions to the magnetic shielding:[83]

$$\delta_{obs} = \sigma - \sigma_0 = (\sigma_{b1} + \sigma_{loca1})\rho = (\sigma_{b1} + \sigma_{ex1} + \sigma_{E1} + \sigma_{a1} + \sigma_{W1} + \sigma_{specific})\rho \quad (2)$$

where σ_{b1} is the contribution from solvent bulk magnetic susceptibility. The local shielding contribution, σ_{loca1}, is a combination of σ_{ex1}, σ_{E1}, $\sigma_{a1,}$ σ_{W1}, and $\sigma_{specific}$, which are contributions from short-range exchange interactions, permanent electronic interactions, magnetic anisotropy, van der Waals dispersion interactions, and specific intermolecular interactions, respectively. According to previous studies, it has been found that σ_{ex1}, σ_{E1}, and σ_{a1} all make negligible contributions in CO_2.[79,84,85] Upon the basis of this work, it is also assumed that all terms except σ_{b1} and σ_{W1} are negligible in He and N_2. The bulk susceptibility contribution to the magnetic shielding constant, σ_{b1}, can be calculated according to[86,87]

$$\sigma_{b1} = -\left(\frac{4}{3}\right)\pi\chi_m \quad (3)$$

where χ_m is the molar magnetic susceptibility. Experimentally, χ_m is measured to be -21.0×10^{-6} cm^3/mol, -12.0×10^{-6} cm^3/mol, and -1.88×10^{-6} cm^3/mol for CO_2, N_2, and He, respectively.[88] This results in σ_{b1} values of 88.0 ppm-cm^3/mol, 50.3 ppm-cm^3/mol, and 7.87 ppm-cm^3/mol for CO_2, N_2, and He, respectively. After subtracting the contribution of the bulk susceptibility, $\sigma_{b1}\rho$, from δ_{obs}, the corrected chemical shift ($\delta_{corrected}$) can be used to obtain the shielding contribution due only to σ_{loca1}. In the present study, σ_{loca1} is assumed to be the result of the combination of van der Waals dispersion interactions and, in the case of the CO_2 complex, any specific intermolecular interactions experienced by the individual nuclei. The resulting line has the general form of

$$\delta_{corrected} = (\sigma_{W1} + \sigma_{specific})\rho \quad (4)$$

in which the slope provides a direct measurement of the contributions to the local shielding parameter from van der Waals and specific interactions. The results for methyl acetate and acetaldehyde are presented in Figure 12, and the tabulated fitting parameters are presented in Table 3.

Small changes in chemical shielding combined with shifts in vibrational wavenumber have been previously used to identify weak C−H···O interactions.[41] As discussed in the Vibrational Spectroscopy section, there are several interaction geometries of comparable energy for each complex that are predicted by the ab initio calculations. Therefore, the resulting electron density redistribution will be a convolution of a system of rapidly exchanging states, making it difficult to predict the degree to which each of the individual protons will be affected. However, the degree to which the compounds interact with the various gases as well as the general trend of the proton interactions can be observed through the slopes of the lines. In the case of He, the slopes fall very close to zero and are within a narrow distribution (5.8 ppm-cm^3/mol). The slopes differ by only 0.6 and 2.4 ppm-cm^3/mol for methyl acetate and acetaldehyde, respectively. This is indicative of very weak, nonspecific interactions between the gas and solute molecules, which is expected for He because it is weakly polarizable and exhibits very weak van der Waals interactions. In N_2, the slopes deviate significantly from zero, indicating some degree of intermolecular interactions. The range of slopes for the various proton signals also remain within a fairly narrow range (3.9

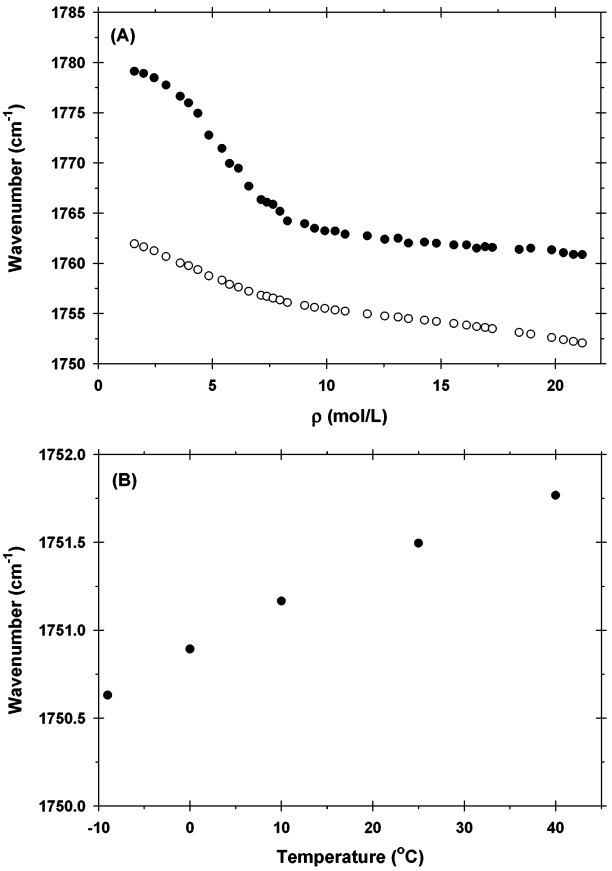

Figure 11. Plots of (A) monomer (●) and complex (○) carbonyl bands of methyl acetate as a function of pressure (345.7−35.4 bars) in supercritical CO_2 at 40.0 °C and (B) the complex band in an isodensity (22.35 mol/L) temperature study (−10.0 to 40.0 °C).

ppm-cm^3/mol), indicating that the deviation from zero is attributable to nonspecific intermolecular interactions that have similar effects on all of the protons in methyl acetate and acetaldehyde. Again, the respective slopes differ only by 2.5 and 4.6 ppm-cm^3/mol. In CO_2, however, the results are dramatically different from those observed in He and N_2. The slopes deviate even further from zero, indicating a substantial intermolecular interaction. However, a more significant result is that the individual proton signals are affected differently. The range in slopes of the four types of protons (18.9 ppm-cm^3/mol) in methyl acetate and acetaldehyde now differ by 4.4 and 12.2 ppm-cm^3/mol; these values are greater than the differences observed for He and N_2 in both cases. This increase in the variation of slopes can be attributed to a specific C−H···O interaction between the solute protons and CO_2.

If the electron redistribution was caused solely by the specific Lewis acid−Lewis base interaction, then one would expect the protons closest to the carbonyl group to be most affected. This is indeed the case for the aldehydic proton compared to the methyl protons in acetaldehyde, both of which are shifted more than either of the proton signals from methyl acetate. Methyl acetate, however, shows the reverse order, with the ester methyl protons being shifted more than the acetate methyl protons. Although this at first may seem puzzling, a closer examination of the ab initio vibrational wavenumber shifts for methyl acetate in Table 2 may provide the explanation. According to these calculations, the cooperative C−H···O interaction in either of the two predicted geometries affect the two methyl groups differently. It can be seen from the wavenumber shifts that the ester methyl group experiences a much more dramatic shift in its vibrational wavenumber than does the acetate methyl. This means that the ester methyl experiences a greater decrease in its bond length and local electronic environment, which would result in a greater degree of shifting compared to that of the acetate methyl protons in the observed NMR measurements.

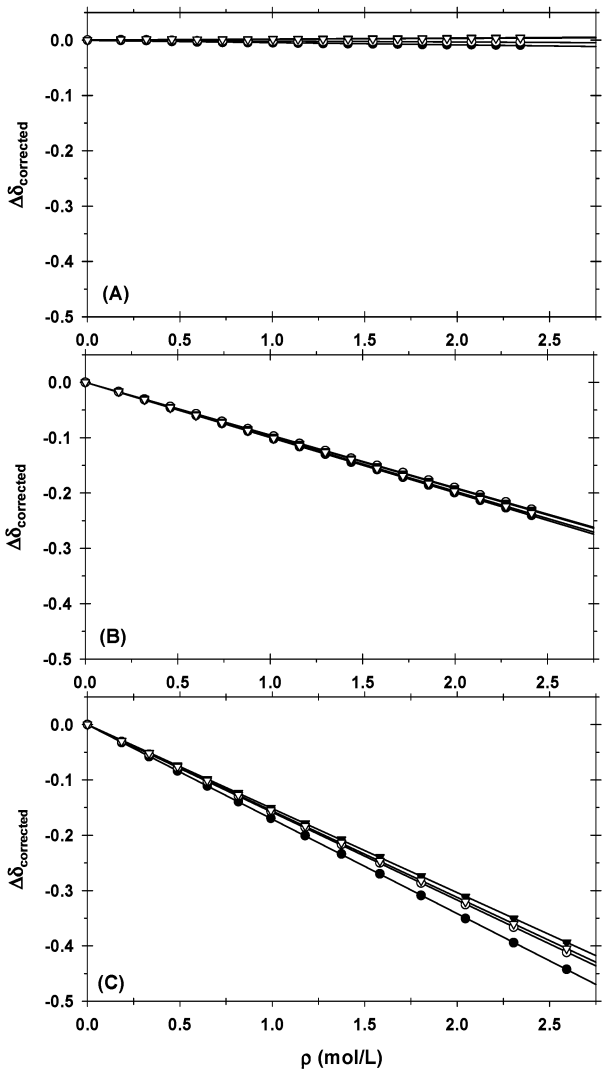

Figure 12. Plots of $\Delta\delta_{corrected}$ vs ρ for acetaldehyde and methyl acetate at 25.0 °C in pressurized (A) He (59.6−1.0 bars), (B) N_2 (59.6−1.0 bars), and (C) CO_2 (45.8−1 bars) for methyl acetate C−CH_3 (▼), methyl acetate O−CH_3 (▽), acetaldehyde C−CH_3 (●), and acetaldehyde C−H (○).

TABLE 3: Fitting Parameters for Plots of $\delta\sigma$[a]

gas	He	N_2	CO_2
methyl acetate CH_3 slope (R^2)	1.9 (0.9720)	−95.9 (0.9999)	−151.9 (1.000)
methyl acetate OCH_3 slope (R^2)	1.3 (0.9000)	−98.4 (0.9999)	−156.3 (0.9999)
acetaldehyde CH_3 slope (R^2)	−1.5 (0.9815)	−95.2 (1.000)	−158.6 (1.000)
acetaldehyde CH slope (R^2)	−3.9 (0.9676)	−99.8 (1.000)	−170.8 (1.000)

[a] Slope units are in ppm-cm^3/mol.

4. Conclusions

In this work, a comprehensive spectroscopic examination of the weak cooperative C−H···O interaction in CO_2−carbonyl complexes as well as the previously known Lewis acid−Lewis

base interaction was undertaken. The vibrational red shifts observed for the carbonyl bands at higher gas densities clearly show the Lewis acid−Lewis base interaction between CO_2 and the carbonyl group. The verification of this interaction is important because it is a necessary condition for the formation of the weaker cooperative interaction. Methyl acetate−CO_2 dilution studies provide further evidence of this stronger specific interaction by demonstrating an equilibrium between monomeric and CO_2−complexed states that shifts toward the complexed state as solvent concentration is increased. No substantial shifting in this equilibrium is observed when He or N_2 is used as the pressurizing medium. The vibrational and NMR spectroscopic results presented here provide strong evidence for the existence of the weak C−H···O interactions in the model carbonyl systems. Blue shifts are observed in both gaseous and supercritical CO_2 for several of the C−H vibrational modes, including the acetaldehyde aldehydic proton and the ν_2 and ν_{19} methyl acetate modes, as predicted by our computational studies. These blue shifts are absent or insignificant in the noninteracting gases, indicating that the changes are not due to solvent density effects and that CO_2 is indeed interacting specifically with these protons. Isodensity temperature studies confirm that the degree of shifting increases as temperature decreases, indicating that the interactions become more significant with respect to kT as the internal energy of the system is lowered. Because the interaction geometries have closely spaced interaction energies, any measurements made at room temperature, either vibrational or NMR, will be a convolution of rapidly exchanging states, making it difficult to predict the final solvation effect on each vibration or shielding constant conclusively. Confirmation of the effects caused by the individual geometries will require more detailed experimentation and analysis. Supersonic jet expansion spectroscopic studies may be able to achieve this objective and provide a better comparison with calculated frequency shifts by producing interaction complexes at extremely low temperatures. NMR measurements show that in CO_2 each proton experiences a significantly larger change in its local magnetic shielding environment as compared to N_2 and He. These variable changes are attributed to the different degrees of electron density redistribution caused by the various interaction geometries predicted for the CO_2 complexes. The data presented here provide strong evidence for the existence of cooperative C−H···O interaction in acetate complexes and show that these interactions are relevant to understanding solvation mechanisms under gaseous and supercritical conditions. Although these measurements were performed on small, model compounds for comparison with the ab initio calculations, we believe that this interaction can be generally applied to all acetate-containing compounds and in the case of peracetylated carbohydrates can be used to help explain their enhanced solubility in CO_2.

Acknowledgment. This material is based upon work supported in part by the STC program of the National Science Foundation under agreement no. CHE-9876674, a Pfizer Analytical Graduate Fellowship (M.A.B.), Merck & Co., Inc., and a Department of Education GAANN Fellowship. We gratefully acknowledge Dr. Stephen Vaughan and Thermo Nicolet for the use of the Magna-IR 750 spectrometer as well as Varian NMR, Inc.

References and Notes

(1) Laintz, K. E.; Wai, C. M.; Yonker, C. R.; Smith, R. D. *J. Supercrit. Fluids* **1991**, *4*, 194−198.
(2) DeSimone, J. M.; Guan, Z.; Elsbernd, C. S. *Science* **1992**, *257*, 945−947.
(3) Rindfleisch, F.; DiNoia, T. P.; McHugh, M. A. *J. Phys. Chem.* **1996**, *100*, 15581−15587.
(4) Sarbu, T.; Styranec, T.; Beckman, E. J. *Nature* **2000**, *405*, 165−168.
(5) Raveendran, P.; Wallen, S. L. *J. Am. Chem. Soc.* **2002**, *124*, 12590−12599.
(6) Raveendran, P.; Wallen, S. L. *J. Phys. Chem. B* **2003**, *107*, 1473−1477.
(7) Kauffman, J. F. *J. Phys. Chem. A* **2001**, *105*, 3433−3442.
(8) Reynolds, L.; Gardecki, J. A.; Frankland, S. J. V.; Horng, M. L.; Maroncelli, M. *J. Phys. Chem.* **1996**, *100*, 10337−10354.
(9) Kazarian, S. G.; Vincent, M. F.; Bright, F. V.; Liotta, C. L.; Eckert, C. A. *J. Am. Chem. Soc.* **1996**, *118*, 1729−1736.
(10) Nelson, M. R.; Borkman, R. F. *J. Phys. Chem. A* **1998**, *102*, 7860−7863.
(11) Meredith, J. C.; Johnston, K. P.; Seminario, J. M.; Kazarian, S. G.; Eckert, C. A. *J. Phys. Chem.* **1996**, *100*, 10837−10848.
(12) Raveendran, P.; Wallen, S. L. *J. Am. Chem. Soc.* **2002**, *124*, 7274−7275.
(13) Pimentel, G. C.; McClellan, A. L. *The Hydrogen Bond*; W. H. Freeman and Company: San Francisco, 1960.
(14) Glasstone, S. *Trans. Faraday Soc.* **1937**, *33*, 200−214.
(15) Sutor, D. J. *J. Chem. Soc.* **1963**, 1105−1110.
(16) Taylor, R.; Kennard, O. *J. Am. Chem. Soc.* **1982**, *104*, 5063−5070.
(17) Schroetter, S.; Bougeard, D.; Schrader, B. *Spectrosc. Lett.* **1985**, *18*, 153−166.
(18) Allerhand, A.; Schleyer, P. v. R. *J. Am. Chem. Soc.* **1963**, *85*, 1715−1723.
(19) Creswell, C. J.; Allred, A. L. *J. Am. Chem. Soc.* **1963**, *85*, 1723−1726.
(20) Paulson, S. L.; Barnes, A. J. *J. Mol. Struct.* **1982**, *80*, 151−158.
(21) Fraser, G. T.; Lovas, F. J.; Suenram, R. D.; Nelson, D. D., Jr.; Klemperer, W. *J. Chem. Phys.* **1986**, *84*, 5983−5988.
(22) DeLaat, A. M.; Ault, B. S. *J. Am. Chem. Soc.* **1987**, *109*, 4232−4236.
(23) Fraser, G. T.; Leopold, K. R.; Klemperer, W. *J. Chem. Phys.* **1984**, *80*, 1423−1426.
(24) Peterson, K. I.; Klemperer, W. *J. Chem. Phys.* **1984**, *81*, 3842−3845.
(25) Peterson, K. I.; Klemperer, W. *J. Chem. Phys.* **1986**, *85*, 725−732.
(26) Dulmage, W. J.; Lipscomb, W. N. *Acta Crystallogr.* **1951**, *4*, 330−334.
(27) Truscott, C. E.; Ault, B. S. *J. Phys. Chem.* **1984**, *88*, 2323−2329.
(28) Fraser, G. T.; Leopold, K. R.; Nelson, D. D., Jr.; Tung, A.; Klemperer, W. *J. Chem. Phys.* **1984**, *80*, 3073−3077.
(29) Bach, S. B. H.; Ault, B. S. *J. Phys. Chem.* **1984**, *88*, 3600−3604.
(30) Dougill, M. W.; Jeffrey, G. A. *Acta Crystallogr.* **1953**, *6*, 831−837.
(31) Desiraju, G. R. *Angew. Chem., Int. Ed. Engl.* **1995**, *34*, 2311−2327.
(32) Desiraju, G. R. *Acc. Chem. Res.* **1996**, *29*, 441−449.
(33) Desiraju, G.; Steiner, T. *The Weak Hydrogen Bond: Applications to Structural Chemistry and Biology*; Oxford University Press: Oxford, U.K., 1999.
(34) Steiner, T. *Crystallogr. Rev.* **1996**, *6*, 1−51.
(35) Wahl, M. C.; Sundaralingam, M. *Trends Biochem. Sci.* **1997**, *22*, 97−102.
(36) Auffinger, P.; Westhof, E. *J. Mol. Biol.* **1997**, *274*, 54−63.
(37) Steiner, T. *J. Phys. Chem. A* **2000**, *104*, 433−435.
(38) Astrup, E. E.; Aomar, A. M. *Acta Chem. Scand., Ser. A* **1975**, *29*, 794−798.
(39) Perchard, J. P.; Perchard, C.; Burneau, A.; Limouzi, J. *J. Mol. Struct.* **1978**, *47*, 285−290.
(40) Jedlovszky, P.; Turi, L. *J. Phys. Chem. B* **1997**, *101*, 5429−5436.
(41) Mizuno, K.; Ochi, T.; Shindo, Y. *J. Chem. Phys.* **1998**, *109*, 9502−9507.
(42) Raymo, F. M.; Bartberger, M. D.; Houk, K. N.; Stoddart, J. F. *J. Am. Chem. Soc.* **2001**, *123*, 9264−9267.
(43) Melikova, S. M.; Rutkowski, K. S.; Rodziewicz, P.; Koll, A. *Chem. Phys. Lett.* **2002**, *352*, 301−310.
(44) Kariuki, B. M.; Harris, K. D. M.; Philp, D.; Robinson, J. M. A. *J. Am. Chem. Soc.* **1997**, *119*, 12679−12680.
(45) Langner, R.; Zundel, G.; Brzezinski, B. *Spectrochim. Acta, Part A* **1999**, *55*, 35−41.
(46) Yoshida, H.; Harada, T.; Murase, T.; Ohno, K.; Matsuura, H. *J. Phys. Chem. A* **1997**, *101*, 1731−1737.
(47) Hobza, P.; Spirko, V.; Selzle, H. L.; Schlag, E. W. *J. Phys. Chem. A* **1998**, *102*, 2501−2504.
(48) Cubero, E.; Orozco, M.; Hobza, P.; Luque, F. J. *J. Phys. Chem. A* **1999**, *103*, 6394−6401.
(49) Hobza, P.; Spirko, V.; Havlas, Z.; Buchhold, K.; Reimann, B.; Barth, H.-D.; Brutschy, B. *Chem. Phys. Lett.* **1999**, *299*, 180−186.
(50) Hobza, P.; Havlas, Z. *Chem. Phys. Lett.* **1999**, *303*, 447−452.

(51) Gu, Y.; Kar, T.; Scheiner, S. *J. Am. Chem. Soc.* **1999**, *121*, 9411−9422.
(52) Masella, M.; Flament, J.-P. *J. Chem. Phys.* **1999**, *110*, 7245−7255.
(53) Wu, D. Y.; Ren, Y.; Wang, X.; Tian, A. M.; Wong, N. B.; Li, W.-K. *THEOCHEM* **1999**, *459*, 171−176.
(54) Hobza, P.; Havlas, Z. *Chem. Rev.* **2000**, *100*, 4253−4264.
(55) Hobza, P.; Sponer, J.; Cubero, E.; Orozco, M.; Luque, F. J. *J. Phys. Chem. B* **2000**, *104*, 6286−6292.
(56) Scheiner, S.; Gu, Y.; Kar, T. *THEOCHEM* **2000**, *500*, 441−452.
(57) Reimann, B.; Buchhold, K.; Vaupel, S.; Brutschy, B.; Havlas, Z.; Spirko, V.; Hobza, P. *J. Phys. Chem. A* **2001**, *105*, 5560−5566.
(58) Hobza, P. *Phys. Chem. Chem. Phys.* **2001**, *3*, 2555−2556.
(59) Scheiner, S.; Grabowski, S. J.; Kar, T. *J. Phys. Chem. A* **2001**, *105*, 10607−10612.
(60) van der Veken, B. J.; Herrebout, W. A.; Szostak, R.; Shchepkin, D. N.; Havlas, Z.; Hobza, P. *J. Am. Chem. Soc.* **2001**, *123*, 12290−12293.
(61) Scheiner, S.; Kar, T. *J. Phys. Chem. A* **2002**, *106*, 1784−1789.
(62) Hartmann, M.; Wetmore, S. D.; Radom, L. *J. Phys. Chem. A* **2001**, *105*, 4470−4479.
(63) Li, X.; Liu, L.; Schlegel, H. B. *J. Am. Chem. Soc.* **2002**, *124*, 9639−9647.
(64) Lemmon, E. W.; McLinden, M. O.; Friend, D. G. In *NIST Chemistry WebBook*; NIST Standard Reference Database Number 69; National Institute of Standards and Technology: Gaithersburg, MD, July 2001.
(65) Blatchford, M. A.; Wallen, S. L. *Anal. Chem.* **2002**, *74*, 1922−1927.
(66) Carter, D. A.; Thompson, W. R.; Taylor, C. E.; Pemberton, J. E. *Appl. Spectrosc.* **1995**, *49*, 1561−1576.
(67) Blatchford, M. A.; Raveendran, P.; Wallen, S. L. *J. Am. Chem. Soc.* **2002**, *124*, 14818−14819.
(68) de Matas, M.; Edwards, H. G. M.; Lawson, E. E.; Shields, L.; York, P. *J. Mol. Struct.* **1998**, *440*, 97−104.
(69) Karger, N.; da Costa, A. M. A.; Ribeiro-Claro, P. J. A. *J. Phys. Chem. A* **1999**, *103*, 8672−8677.
(70) Marques, M. P. M.; da Costa, A. M. A.; Ribeiro-Claro, P. J. A. *J. Phys. Chem. A* **2001**, *105*, 5292−5297.
(71) Bowman, L. E.; Palmer, B. J.; Garrett, B. C.; Fulton, J. L.; Yonker, C. R.; Pfund, D. M.; Wallen, S. L. *J. Phys. Chem.* **1996**, *100*, 18327−18334.
(72) George, W. O.; Houston, T. E.; Harris, W. C. *Spectrochim. Acta, Part A* **1974**, *30*, 1035−1057.
(73) Hollenstein, H.; Guenthard, H. H. *Spectrochim. Acta, Part A* **1971**, *27*, 2027−2060.
(74) Bellamy, L. J. *Advances in Infrared Group Frequencies*; Methuen: London, 1968.
(75) Myers, D. J.; Shigeiwa, M.; Fayer, M. D.; Cherayil, B. J. *Chem. Phys. Lett.* **1999**, *313*, 592−599.
(76) Myers, D. J.; Shigeiwa, M.; Fayer, M. D.; Cherayil, B. J. *J. Phys. Chem. B* **2000**, *104*, 2402−2414.
(77) Myers, D. J.; Shigeiwa, M.; Cherayil, B. J.; Fayer, M. D. *J. Chem. Phys.* **2001**, *115*, 4689−4695.
(78) Jameson, C. J. *Chem. Rev.* **1991**, *91*, 1375−1395.
(79) Trappeniers, N. J.; Oldenziel, J. G. *Physica A* **1975**, *82*, 581−595.
(80) Yonker, C. R.; Zemanian, T. S.; Wallen, S. L.; Linehan, J. C.; Franz, J. A. *J. Magn. Reson., Ser. A* **1995**, *113*, 102−107.
(81) Wallen, S. L.; Palmer, B. J.; Garrett, B. C.; Yonker, C. R. *J. Phys. Chem.* **1996**, *100*, 3959−3964.
(82) Linehan, J. C.; Wallen, S. L.; Yonker, C. R.; Bitterwolf, T. E.; Bays, J. T. *J. Am. Chem. Soc.* **1997**, *119*, 10170−10177.
(83) Pfund, D. M.; Zemanian, T. S.; Linehan, J. C.; Fulton, J. L.; Yonker, C. R. *J. Phys. Chem.* **1994**, *98*, 11846−11857.
(84) Lim, Y. H.; Nugara, N. E.; King, A. D., Jr. *J. Phys. Chem.* **1993**, *97*, 8816−8819.
(85) Jameson, C. J.; De Dios, A. C. *J. Chem. Phys.* **1992**, *97*, 417−434.
(86) Bennett, B.; Raynes, W. T. *Magn. Reson. Chem.* **1991**, *29*, 946−954.
(87) Smith, A.; Raynes, W. T. *J. Crystallogr. Spectrosc. Res.* **1983**, *13*, 77−87.
(88) *CRC Handbook of Chemistry and Physics*, 83 ed.; Lide, D. R., Ed.; CRC Press: Boca Raton, FL, 2002.